organic extract was evaporated *in vacuo* to yield a crude extract, which was subjected repeatedly to silica gel column chromatography using *n*-hexane–ethyl acetate as the solvent.

Cell Culture and 96-Well Based Assay Procedures—Primary neuronal cells were prepared from embryonic 17-d Wister rat brains as described by Suzumura *et al.* (*27*). In brief, the meninges were removed and the brains were dissociated by adding in Dulbecco's modified Eagle's medium (DMEM) MIXTURE F-12 HAM (Sigma Aldrich Fine Chemicals, St. Louis, MO, USA) containing 2.85 mg/ml glucose, 5 μM HEPES, 25 μg/ml insulin, 2 μM progesterone, 0.1 mM putrescine, 0.03 μM sodium selenite, 0.1 mg/ml apo-transferrin, 100 U/ml penicillin and 100 μg/ml streptomycin (DF medium).

For screening microbial metabolites, primary neuronal cells were cultured on poly-D-lysine (PDL) coated 96-well plastic plates (Becton Dickinson, NJ, USA) at an initial density of 0.7×10^5 cells/cm^2 in 2% fetal bovine serum (FBS)–DF medium for 5 d at 37°C. The cultures were treated with microbial metabolites for 24 h, and then, cell death was induced by adding 1 mM SIN-1 (Dojindo, Kumamoto Japan) or 4 μg/ml DDC (Wako, Osaka, Japan). After 24 h, and live cells were counted using a Cell Counting Kit-8 (Dojindo). The kit detects mitochondrial NADH-dehydrogenase activity in live cells by measuring the reduction of the tetrazolium monosodium salt, WST-8. This is a modified MTT assay, and it is known that the MTT assay is not influenced in the presence of various oxidants. Cell number was also measured by the CyQUANT Cell Proliferation Assay Kit (Molecular Probes, Eugene, USA), which quantifies the amount of DNA (*28*). The chemical structures of the compounds obtained were determined by NMR analysis.

PC12 cells were incubated in 75-cm^2 tissue culture flasks in DMEM (Nissui, Tokyo, Japan) supplemented with 10% FBS, 5% horse serum (HS), 100 U/ml penicillin, and 100 μg/ml streptomycin. NGF-differentiated PC12 cells were treated with 100 ng/ml NGF for 5 d. Cells of the rat fibroblast cell line 3Y1 were cultured in DMEM containing 10% FBS, 100 U/ml penicillin, and 100 μg/ml streptomycin.

To study the protective effects of microbial metabolites and known scavengers on PC12 cells and 3Y1 cells, cells were cultured at a initial density of 3.0×10^3 cells/cm^2 in DMEM supplemented with 10% FBS, 5% HS or DMEM containing 10% FBS 5 d at 37°C. Cell death induced by SIN-1 and cell viability were measured as described above.

All cultures were maintained at 37°C in a humidified CO_2-incubator.

Observation of Tyrosine Nitration by Immunofluorescence—Primary neuronal cells were cultured for 7 d on PDL-coated 8-well culture slides (Becton Dickinson). The cells were fixed with 4% paraformaldehyde in PBS (+) (phosphate-buffered saline containing 0.9 mM Ca^{2+} and 0.5 mM Mg^{2+}) for 1 h, washed three times with PBS (+), and incubated with 10% FBS-PBS (+) at 4°C for 1 h. Next, they were incubated with an anti-nitrotyrosine antibody 1AE (Upstate, VA, USA) in 10% FBS-PBS (+) at 4°C for 1 h. After two washes with PBS (+), the cells were incubated with fluorescein isothiocyanate (FITC)-conjugated goat anti-mouse IgG (H&L) (ICN Pharmaceuticals, Inc. Morgan, Irvine, CA, USA) in 10% FBS-PBS (+) for 1 h. Cell nuclei were stained with 10 μg/ml of 4′,6-diamidino-2-phenylindole (DAPI) (Sigma Aldrich Fine Chemicals) at 37°C for 30 min. The cells were then washed with PBS (+), and the nuclear DNA was observed under a fluorescence microscope IX70 (OLYMPUS, Tokyo, Japan).

Measurement of Scavenging Activity—We measured $ONOO^-$ and O_2^- scavenging activities using the chemiluminescent procedure described by Radi *et al.* (*29*) and Beauchamp and Fridovich (*30*), respectively. In brief, 400 mM 5-amino-2,3-dihydro-1,4-phthalazinedione (luminol) (Sigma Aldrich Fine Chemicals) was diluted with 5 mM $NaHCO_3$, pH 10.5 (Wako) in Hank's balanced salt solution (HBSS) (Invitrogen Corp, Carlsbad, CA, USA) (solution A). Test compounds were diluted with HBSS (pH 7.0) (solution B). Solutions A and B and 0.5 mM SIN-1 diluted with HBSS (pH 7) were mixed, and then $ONOO^-$ was measured using a chemiluminometer (MicroLumat LB96V; Berthold Technology, Bad Wildbad, Germany) for 20 min. O_2^- was generated by the xanthine-xanthine oxidase system following the modified method of Beauchamp and Fridovich (*30*). Specimens in Tris-HCl buffer were added to the wells of 96-well plates, each well containing 10 U/ml xanthine oxidase and 2 μM 2-methyl-6-(*p*-methoxyphenyl)-3,7-dihydriimidazo-[1,2-α]pyrazin-3-one (MCLA; Tokyo Kasei Co. Ltd, Tokyo, Japan). To generate O_2^-, 30 μM xanthine was added to each well. Chemiluminescence intensity was measured with a chemiluminometer for 10 min. NO scavenging activity was measured by the fluorometric method of Kojima *et al.* (*31*). The fluorometric detection of NO was carried out using the NO indicator (NONOate; Dojindo) and diaminofluorescein-2 (DAF-2; Daiichi Pure Chemicals Co. Ltd, Tokyo, Japan). The fluorescence from DAF-2T, the reaction product of DAF-2 with NO, was measured as the fluorescence intensity of DAF-2T using a microplate fluorescence reader (Packard Instrument Co., Meriden, USA) (Ex = 490 nm and Em = 520 nm). Mn-TBAP (Dojindo), a scavenger of $ONOO^-$ and O_2^-, and 2-(4-carboxyphenyl)-4,4,5,5-tetramethylimidazoline-1-oxyl 3-oxide (C-PTIO, Dojindo), a scavenger for NO, were used as controls.

Caspase Activity Assay—We measured caspase-3 activity according to Zhou *et al.* (*32*). After exposure to $ONOO^-$, cells were incubated in 50 mM Tris-HCl buffer (pH7.4) containing 4 mM DTT (Sigma Aldrich Fine Chemicals), 2 mM EDTA, 10% glycerol, 0.1% Triton X-100 and 20 μM Ac-Asp-Glu-Val-Asp-7-amido-4-methylcoumarine (Sigma Aldrich Fine Chemicals), a fluorogenic substrate for caspase-3. The activity of caspase-3-like proteases was determined by measuring the fluorescence intensity of the cleaved substrate in a microplate fluorescence reader (Packard Instrument Co., Meriden, USA) (Ex = 360 nm and Em = 460 nm).

RESULTS

Screening of Microbial Metabolites That Prevent SIN-1-Induced Neuronal Cell Death—We screened two hundred microbial metabolites and obtained one compound that rescued primary neuronal cells from SIN-1-induced death. This compound was identified as neoechinulin A by NMR analysis. In the presence of SIN-1, the viability

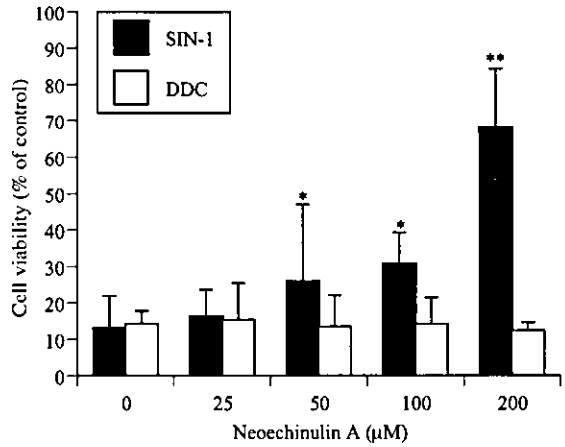

Fig. 1. **Dose-dependent effects of neoechinulin A on neuronal cells.** Primary neuronal cells were seeded at a density of 1.4×10^5 cells/cm^2. After 5 d, cells were incubated with neoechinulin A for 24 h, and treated with 1 mM SIN-1 or 4 μg/ml DDC for 24 h. Cell viability was measured using a Cell Counting Kit-8 (means ± SD, n = 4). $^*p < 0.05$, $^{**}p < 0.01$.

of primary neuronal cells was less than 15%. Treatment with 200 μM neoechinulin A increased cell viability to more than 60%, while such treatment provided no protection against cell death induced by DDC (Fig. 1). This indicates that neoechinulin A protects primary neuronal cells against $ONOO^-$-induced death, but not against O_2^--induced death.

3Y1 cells, a fibroblast cell line, were not rescued from SIN-1–induced death by neoechinulin A. To determine the protective specificity of neoechinulin A, its effect on NGF-differentiated and undifferentiated PC12 cells was examined. Neoechinulin A rescued only differentiated PC12 cells (Fig. 2), suggesting that protective properties of the compound are specific to neuronal cells. Differentiated PC12 cells were also dose-dependently rescued by neoechinulin A (Fig. 3.). The results, shown in the Figures 2 and 3, were confirmed using another cell counting kit, the CYQUANT Cell proliferation kit (data not shown).

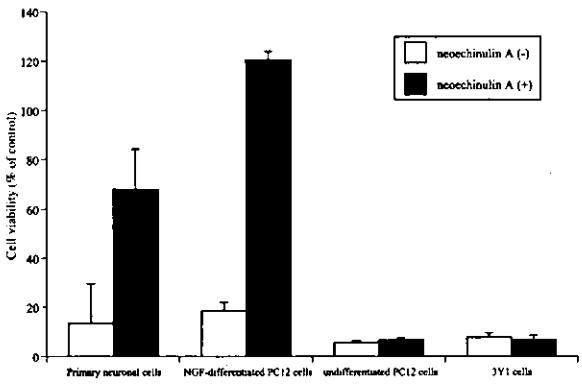

Fig. 2. **Preventive effect of neoechinulin A against SIN-1 injury.** Primary neuronal cells (1.4×10^5 cells/cm^2), PC12 cells (3.0×10^3 cells/cm^2) and 3Y1 cells (3.0×10^3 cells/cm^2) were cultured on PDL-coated 96-well plates for 5 d. After treatment with or without 200 μM neoechinulin A for 24 h, cells were cultured in the presence of 1 mM SIN-1 for 24 h. Cell viability was determined using a Cell Counting Kit-8.

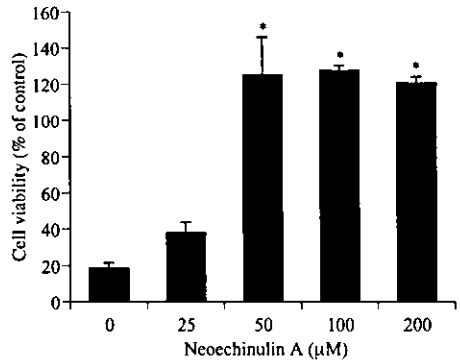

Fig. 3. **Dose-dependent effects of neoechinulin A on differentiated PC12 cells.** PC12 cells were seeded at a density of 3.0×10^3 cells/cm^2 and treated with 100 ng/ml NGF for days. Differentiated PC12 cells were incubated with neoechinulin A for 24 h, and treated with 1 mM SIN-1 for 24 h. Cell viability was measured using a Cell Counting Kit-8. (means ± SD, n = 4) $^*p < 0.01$.

Ability of Neoechinulin A to Scavenge ROS Produced by SIN-1—To study the scavenging activity of neoechinulin A, we examined the nitration of tyrosine residues in SIN-1–exposed cells by immunostaining with monoclonal anti-nitrotyrosine antibody 1AE. Tyrosine nitration was almost completely inhibited by neoechinulin A (Fig. 4), suggesting that neoechinulin A has $ONOO^-$ scavenging activity. This activity was confirmed by the chemiluminescence procedure. The $ONOO^-$ scavenging activity of neoechinulin A is comparable to the activities of Mn-TBAP and C-PTIO (Fig. 5A). Scavenging either O_2^- or NO also prevents the generation of $ONOO^-$ from SIN-1. Mn-TBAP and SOD scavenge about 100% and 75%, respectively of O_2^-, while neoechinulin A does not scavenge O_2^- (Fig. 5B). The fluorometric procedure using DAF-2 revealed that C-PTIO scavenges about 60% of NO, while neoechinulin A does not eliminate NO (Table 1). These results indicate that neoechinulin A specifically scavenges $ONOO^-$, but not O_2^- and NO.

Neuroprotective Effects of Neoechinulin A in SIN-1-Induced Oxidative Stress—It has been reported that various substances, such as anti-apoptotic compounds and neurotrophic factors, have neuroprotective activities (*33*, *34*). We confirmed the neuroprotective effect of the scavengers, C-PTIO and uric acid (Fig. 6A). To examine the activities of neoechinulin A other than scavenging activity, differentiated PC12 cells were pretreated with neoechinulin A, C-PTIO and uric acid for 24 h, and then, after removal of the compounds, with SIN-1 for 24 h. Under these conditions, the scavengers did not rescue differentiated PC12 cells. As shown in Fig. 6B, neoechinulin A still had a neuroprotective effect. This result suggests that neoechinulin A activities other than its scavenging activity.

Figure 3 shows that the viability of neoechinulin A–treated cells was increased by 120%. In this study, live cells were counted with a cell counting kit that measures NADH-dehydrogenase activity as described in "MATERIALS AND METHODS." Several researchers have reported that NGF and bFGF increase the mitochondrial NADH-

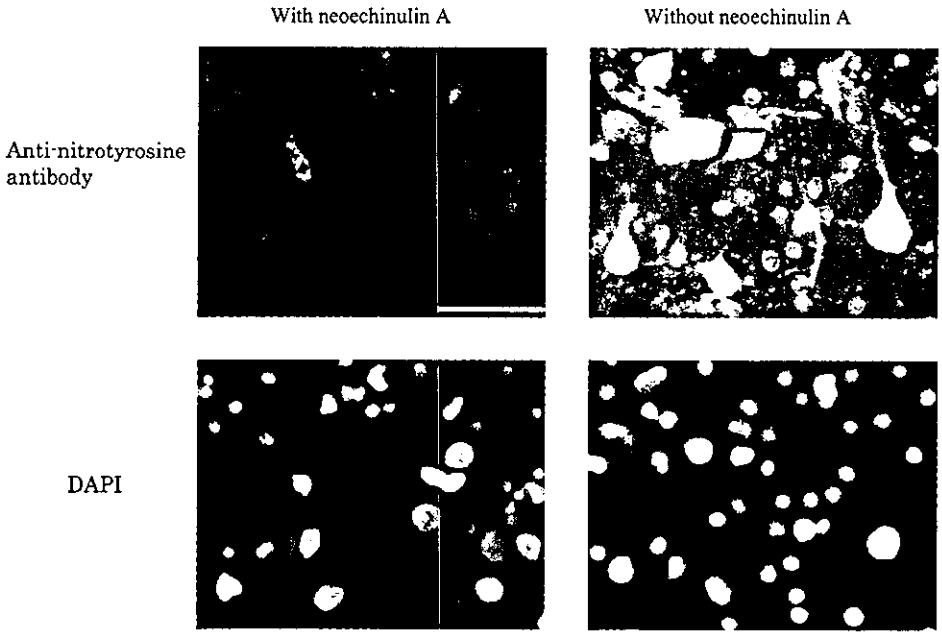

Fig. 4. **Prevention of $ONOO^-$-induced tyrosine nitration by neoechinulin A.** Primary neuronal cells were incubated with 0.25 mM SIN-1 for 2 h with or without 200 μM neoechinulin A, and stained with an anti-nitrotyrosine antibody 1AE and DAPI as described in "MATERIALS AND METHODS." Bar = 50 μm

dehydrogenase activity of PC12 cells (*35*, *36*). These facts suggest that neoechinulin A activates this enzyme in PC12 cells. To examine this possibility, we investigated the effect of neoechinulin A on NADH-dehydrogenase in differentiated PC12 cells in the absence of SIN-1. NADH-dehydrogenase activity was normalized to the number of cells as measured with the assay kit that counts cell number based on quantification of genomic DNA. A significant increase in NADH-dehydrogenase activity was observed after the addition of neoechinulin A (Fig. 7).

$ONOO^-$ activates caspase-3 (*37*, *38*). Thus, we examined the effect of neoechinulin A on the SIN-1–induced activation of caspase-3-like proteases in differentiated PC12 cells. The activation was suppressed by about 65% by 200 μM neoechinulin A. On the other hand, neoechinulin A did not influence the caspase-3–ike protease activity of 3Y1 cells (Fig. 8). These results indicate that neoechinulin A has neurotrophic factor-like and anti-apoptotic activities.

DISCUSSION

Neoechinulin A is a known metabolite of *A. rubber* and *A. amstelodami* (*26*). Yagi *et al.* (*39*) reported neoechinulin A to be an antioxidant compound that suppresses lipid peroxidation in dried bonito flakes, *Katsuobushi*. However, additional properties of the compound were not investigated. In this paper, we show that neoechinulin A has scavenging, neurotrophic factor-like and anti-apoptotic activities. The results shown in Fig. 5 and Table 1 indicate that the compond scavenges only $ONOO^-$ released

Table 1. **NO generation in the presence of scavengers.**

Compounds	Generation of NO (% of control)
None	100
Neoechinulin A	100 ± 3
C-PTIO	41 ± 1
SOD	108 ± 5

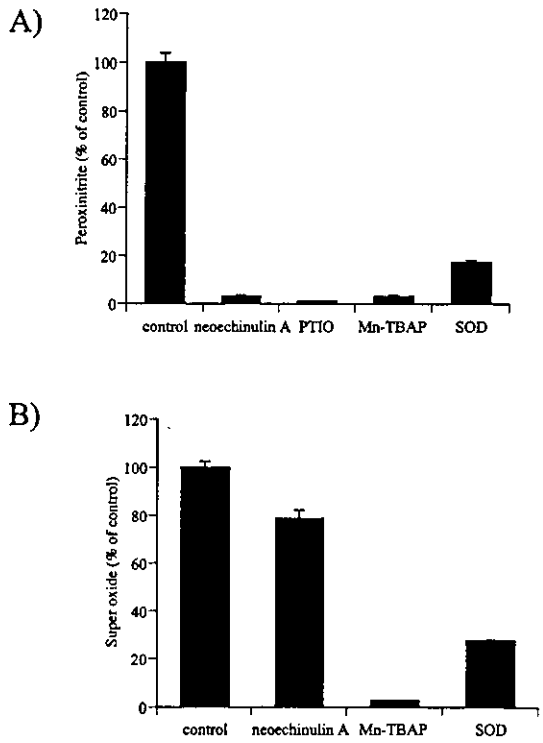

Fig. 5. **Scavenging activity of neoechinulin A.** (A) Measurement of $ONOO^-$ by luminol-dependent chemiluminescence. Luminol was diluted to 400 mM with 5 mM $NaHCO_3$ (pH 10.5) and the samples were diluted with HBSS, pH 7, prior to the measurement of chemiluminescence. Just before measurement, 0.5 mM SIN-1 diluted with HBSS, pH7, was added, and the amount of $ONOO^-$ was measured by a chemiluminometer for 20 min. (B) Measurement of O_2^- by luminol-dependent chemiluminescence. Samples in 100 μl of Tris-HCl buffer, pH 7.4, containing 10 U/ml xanthine oxidase were incubated in a 96-well plate, and 1 μM of MCLA (50 μl) were added. Xanthine (30 μM, 50 μl) was added to generate O_2^-, and the amount of $ONOO^-$ was measured by a chemiluminometer for 20 min.

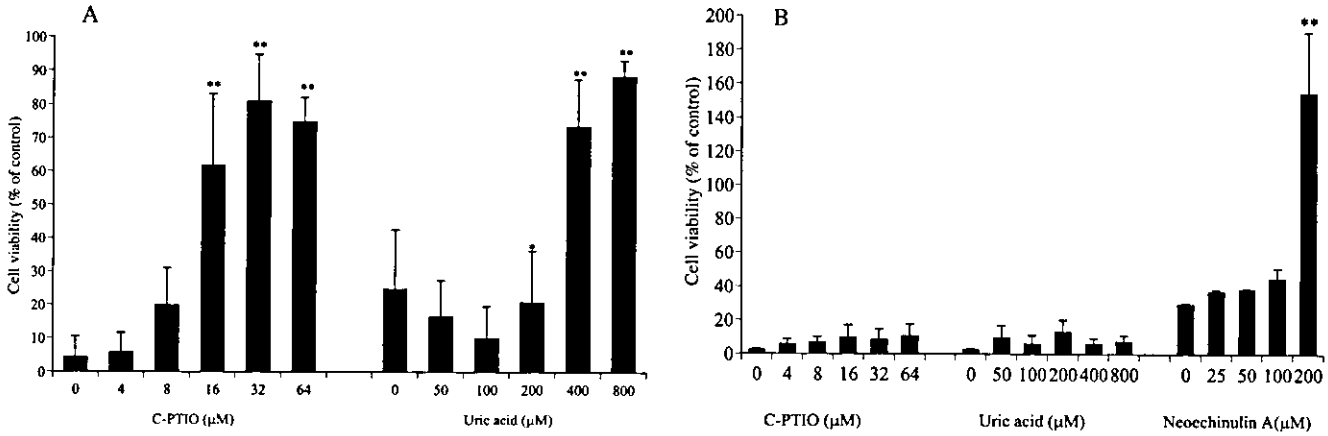

Fig. 6. **Neuroprotective effect of neoechinulin A and scavengers.** PC12 cells were seeded at a density of 3.0×10^3 cells/cm^2 and treated with 100 ng/ml NGF for 5 d. Cell viability was measured using a Cell Counting Kit-8. (A) Cells were incubated with scavengers for 24 h, and treated with 1 mM SIN-1 for 24 h. (B) Cells were incubated with neoechinulin A for 24 h. The neoechinulin A was removed and the cells were treated with 1 mM SIN-1 for 24 h. (means ± SD, $n = 4$) $^*p < 0.05$, $^{**}p < 0.01$.

from SIN-1. In addition, neoechinulin A specifically protects neuronal cells against SIN-1–induced cell death (Fig. 2). Thus, neoechinulin A is very useful for investigations of $ONOO^-$-induced neuronal cell death.

$ONOO^-$ is a powerful oxidant and cytotoxin whose production has been associated with conditions that result in damage to neurons. The appearance of nitrotyrosine immunoreactivity in postmortem brain from individuals with Parkinson's disease and other neurodegenerative conditions (*40–42*) also serves as indirect evidence of $ONOO^-$ production. It is well known that extracts of *Gingko biloba* leaves (EGb 761) rescue neuronal cells against ROS-induced cell death (*43*, 44). EGb 761 includes two major groups of constituents, flavonoids and terpenoids, that are involved in scavenging and anti-apototic activities. It has been reported that EGb 761 increases the level of mRNA for the mtDNA-encoded subunit 1 of NADH-dehydrogenase (*45*) and suppresses the activation of caspase-3 caused by various apoptosis inducers (*46*). In the case of neoechinulin A, one compound has scavenging, neurotrophic factor-like and anti-apoptotic activities. It should be noted that neoechinulin A scavenges $ONOO^-$, but not NO, because NO has various physiological functions (*4–7*). Therefore, neoechinulin A may be useful for protection against $ONOO^-$-induced neuronal cell death in neurodegenerative diseases.

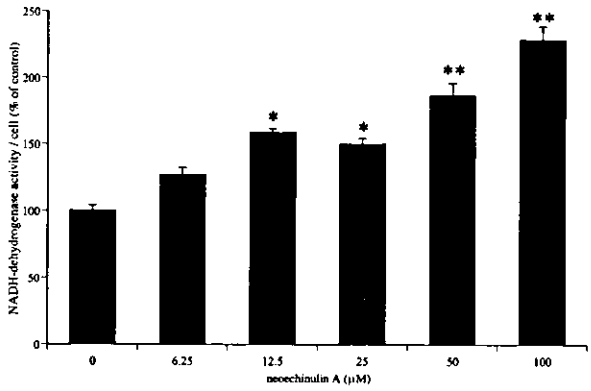

Fig. 7. **Effect of neoechinulin A on the NADH-dehydrogenase activity of PC12 cells.** PC12 cells were seeded at a density of 3.0×10^3 cells/cm^2 and treated with 100 ng/ml NGF for 5 d. The indicated concentration of neoechinulin A was added to each well and the relative NADH-dehydrogenase activity per cell was determined as described in "MATERIALS AND METHODS" (means ± SD, $n = 4$). $^*p < 0.05$, $^{**}p < 0.01$.

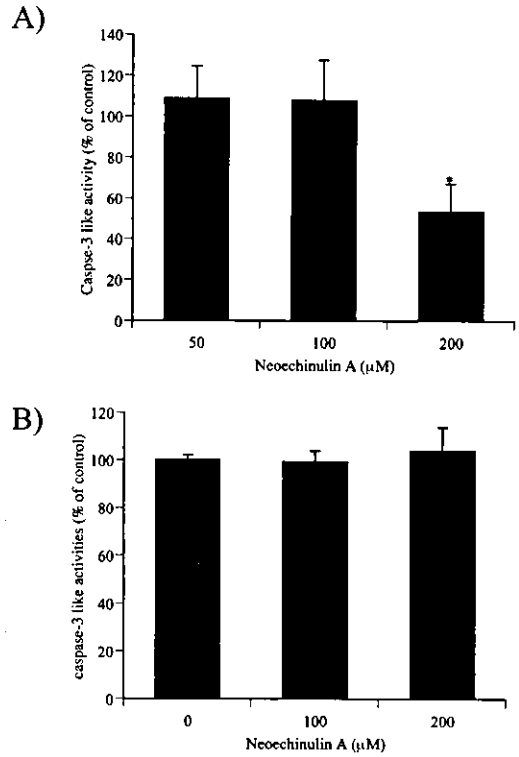

Fig. 8. **Effect of neoechinulin A on caspase-3 like protease activity.** PC12 cells (A) and 3Y1 cells (B) were seeded at a density of 3.0×10^3 cells/cm^2. PC12 cells were treated with 100 ng/ml NGF. Five days later, the cells were incubated with neoechinulin A for 24 h. After removal of the neoechinulin A, 0.5 mM SIN-1 was added. After 3 h, caspase activity was measured as described in "MATERIALS AND METHODS" (means ± SD, $n = 4$). $^*p < 0.01$.

This research was supported in part by grants for Research on Advanced Medical Technology from the Ministry of Health, Labor and Welfare of Japan, and from the Promotion and Mutual Aid Corporation for Private Schools of Japan. We thank Mr. T. Shimada and Miss. Y. Ishihara (Science University of Tokyo) for excellent technical assistance.

REFERENCES

1. Beckman, J.S. (1996) The physiological and pathological chemistry of nitric oxide in *Nitric Oxide* (Lancaster, J.R., ed.) pp.1–82, New York Academic, New York
2. Behl, C., Davis, J.B., Lesley. R., and Schubert, D. (1994) Hydrogen peroxide mediates amyloid beta protein toxicity. *Cell* **77**, 817–827
3. Enokido, Y. and Hatanaka, H. (1993) Apoptotic cell death occurs in hippocampal neurons cultured in a high oxygen atmosphere. *Neuroscience* **57**, 965–972
4. Nathan, C.F. (1992) Nitric oxide as a secretory product of mammalian cells. *FASEB J.* **6**, 3051–3064
5. Schmidt, H.H., Walter, U. (1994) NO at work. *Cell* **78**, 919–925
6. Garthwaite, J. and Boulton, C.L. (1995) Nitric oxide signaling in the central nervous system. *Annu. Rev. Physiol.* **57**, 683–706
7. Yun, H-Y., Dawson, V.L., and Dawson, T.M. (1996) Neurobiology of nitric oxide. *Crit. Rev. Neurobiol.* **10**, 291–316
8. Huang, Z., Huang, P.L., Panahian, N., Dalkara, T., Fishman, M.C., and Moskowitz, M.A. (1994) Effects of cerebral ischemia in mice deficient in neuronal nitric oxide synthase. *Science* **265**, 1883–1885
9. Estévez, A.G., Radi, F., Barbeito, L., Shin, J.T, Thompson, J.A., and Beckman, J.S. (1995) Peroxynitrite-induced cytotoxicity in PC12 cells: evidence for an apoptotic mechanism differentially modulated by neurotrophic factors. *J. Neurochem.* **65**, 1543–1550
10. Troy, C.M., Derossi, D., Prochiantz, A., Greene, L.A., and Shelanski, M.L. (1996) Downregulation of Cu/Zn superoxide dismutase leads to cell death via the nitric oxide-peroxynitrite pathway. *J. Neurosci.* **16**, 253–261
11. Spear, N., Estévez, A.G., Barbeito, L., Beckman, J.S., and Johnson, G.V. (1997) Nerve growth factor protects PC12 cells against peroxynitrite-induced apoptosis via a mechanism dependent on phosphatidylinositol-3 kinase. *J. Neurochem.* **69**, 53–59
12. Bonfoco, E., Krainc, D., Ankarcrona, M., Nicotera, P., and Lipton, S.A. (1995) Apoptosis and necrosis: two distinct events induced, respectively, by mild and intense insults with N-methyl-D-aspartate or nitric oxide/superoxide in cortical cell cultures. *Proc. Natl Acad. Sci. USA* **92**, 7162–7166
13. Torreilles, F., Salman-Tabcheh, S., Guerin, M., and Torreilles, J. (1999) Neurodegenerative disorders: the role of peroxynitrite. *Brain Res. Brain Res. Rev.* **30**, 153–163
14. Radi, R., Beckman, J.S., Bush, K.M., and Freeman, B.A. (1991) Peroxynitrite oxidation of sulfhydryls. The cytotoxic potential of superoxide and nitric oxide. *J. Biol. Chem.* **266**, 4244–4250
15. Ischiropoulos, H., Zhu, L., Chen, J., Tsai, M., Martin, J.C., Smith, C.D., and Beckman, J.S. (1992) Peroxynitrite-mediated tyrosine nitration catalyzed by superoxide dismutase. *Arch. Biol. Chem. Biophys.* **298**, 431–437
16. Smith, M.A., Harris, P.L.R., Sayre, L.M., Beckman, J.S., and Perry, G. (1997) Widespread peroxynitrite-mediated damage in Alzheimer's disease. *J. Neurosci.* **17**, 2653–2657
17. Huie, R.E. and Padmaja, S. (1993) The Reaction of NO with Superoxide. *Free Rad. Res. Commun.* **18**, 195–199
18. Noach, E. and Feelisch, E. (1991) Molecular mechanisms of nitrovasodilator bioactivation. *Basic Res. Cardiol.* **86**, 37–50
19. Trackey, J.L., Uliasz, T.F., and Hewett, S.J. (2001) SIN-1-induced cytotoxicity in mixed cortical cell culture: peroxynitirite-dependent and -independent induction of excitotoxic cell death. *J. Neurochem.* **79**, 445–455
20. Kume, T., Nishikawa, H., Tomioka, H., Katsuki, H., Akaike, A., Kaneko, S., Maeda, T., Kihara, T., and Shimohama, S. (2000) p75-mediated neuroprotection by NGF against glutamate cytotoxicity in cortical cultures. *Brain. Res.* **852**, 279–289
21. Regoli, R. and Winston, G.W. (1999) Quantification of total oxidant scavenging capacity of antioxidants for peroxynitrite, peroxyl radicals, and hydroxyl radicals. *Taxicol. Appl. Pharmacol.* **156**, 96–105
22. Quijano, C., Hernandez-Saavedra, D., Castro, L., McCord, J.M., Freeman, B.A., and Radi, R. (2001) Reaction of peroxynitrite with Mn-superixide dismutase. Role of the metal center in decomposition kinetics and nitration. *J. Biol. Chem.* **276**, 11631–11638
23. Pardo, C.A., Xu, Z., Borchelt, D.R., Price, D.L., Sisodia, S.S., and Cleveland, D.W. (1995) Superoxide dismutase is an abundant component in cell bodies, dendrites, and axons of motor neurons and in a subset of other neurons. *Proc. Natl Acad. Sci. USA* **92**, 954–958
24. Du, J., Suzuki, H., Nagase, F., Akhand, A.A., Ma, X.Y., Yokoyama, T., Miyata, T., Nakashima, .I. (2001) Superoxide-mediated early oxidation and activation of ASK1 are important for initiating methylglyoxal-induced apoptosis process. *Free Radic. Biol. Med.*, **31**, 469–478
25. Cocco, D., Calabrese, L., Rigo, A., Argese, E., and Rotilio, G. (1981) Re-examination of the reaction of diethyldithiocarbamate with the copper of superoxide dismutase. *J. Biol. Chem.*, **256**, 8983–8986
26. Inoue, S., Murata, J., Takamatsu, N., Nagano, H., and Kishi, Y. (1977) Synthetic studies on echinulin and related natural products. V. Isolation, sturucture and synthesis of echinulin-neoechinulin type alkaloids isolated from *Aspergillus amstelodami* (author's transl.). *Yakugaku Zasshi* **97**, 576–581
27. Suzumura, A., Sawada, M., and Marunouti, T. (1996) Selective induction of interleukin-6 in mouse microglia by granulocyte-macrophage colony-stimulating factor. *Brain. Res.* **713**, 192–198
28. Chandrasekher, G., Ma, X., Lallier, T.E., Bazan, and H.E.P. (2002) Delay of corneal epithelial wound healing and induction of keratocyte apoptosis by platelet-activating factor invest. *Ophthalmol. Vis. Sci.* **43**, 1422–1428
29. Radi, R., Cosgrove, T.P., Beckman, J.S., and Freeman, B.A. (1993) Peroxynitrite-induced luminol chemiluminescence. *Biochem. J.* **290**, 51–57
30. Beauchamp, C. and Fridovich, I. (1971) Superoxide dismutase: improved assays and an assay applicable to acrylamide gels. *Anal. Biol.* **44**, 276–287
31. Kojima, H., Nakatsubo, N., Kiuchi, K., Kawahara, S., Kirino, Y., Nagoshi, H., Hirata, Y., and Nagano, T. (1998) Detection and imaging of nitric oxide with novel fluorescent indicators: diaminofluoresceins. *Anal. Chem.* **70**, 2446–2453
32. Zhou, L.J. and Zhu, X.Z. (2000) Reactive oxygen species-induced apoptosis in PC12 cells and protective effect of biobalide. *J. Pharmacol. Exp. Ther.* **293**, 982–988
33. Connner, B. and Dragunow, M. (1998) The role of neuronal growth factors in neurodegenerative disorders of the human brain. *Brain Res. Brain Res. Rev.* **27**, 1–39
34. Satoh, T. (2002) Neurotrophin-like low molecular weight compounds. *Nippon Yakurigaku Zasshi* **120**, 327–334
35. Rhodes, C.H., Nezitis, S.G.E., Gonatas, N.K., and Fleiscier, B. (1989) Selective effect of nerve growth factor on some Golgi and lysosomal enzyme activities of rat pheochromocytoma (PC12) cell. *Arch. Biochem. Biophys.* **272**, 175–184
36. Ohuchi, T., Maruoka, S., Sakudo, A., and Arai, T. (2002) Assay-based quantitative analysis of PC12 cell differentiation. *J. Neurosci. Methods* **118**, 1–8
37. Bao, F. and Liu, D. (2003) Peroxynitrite generated in the rat spinal cord induces apoptotic cell death and activates caspase-3. *Neuroscience* **116**, 59–70
38. Ito, S., Wu, G., Kimoto, T., Hisatomi, T., Ishibashi, T., Rao, N. (2004) Peroxynitrite-induced apoptosis in photoreceptor cells. *Curr. Eye Res.* **28**, 17–24
39. Yagi, Y. and Doi, M. (1999) Isolation of an antioxidative substance produced by *Aspergillus repens*. *Biosci. Biotechnol. Biochem.* **63**, 932–933

40. Good, P.F., Werner, P., Hsu, A., Olanow, C.W., and Perl, D.P. (1996) Evidence of neuronal oxidative damage in Alzheimer's disease. *Am. J. Pathol.* **149**, 21–28
41. Good, P.F., Hsu, A., Werner, P., Perl, D.P., and Olanow, C.W. (1998) Protein nitration in Parkinson's disease. *J. Neuropathol. Exp. Neurol.* **57**, 338–342
42. Heales, S.J., Bolanos, J.P., Stewart, V.C., Brookes, P.S., Land, J.M., and Clark, J.B. (1999) Nitric oxide, mitochondria and neurological disease. *Biochim. Biophys. Acta* **1410**, 215–228
43. Marcocci, L., Maguire, J.J., Droy-Lefaix, M.T., and Paker, L. (1994) The nitric oxide-scavenging properties of *Gingko biloba* extract EGb 761. *Biochem. Biophys. Res. Commun.* **201**, 462–475
45. Marcocci, L., Paker, L., Droy-Lefaix, M.T., Sakaki, A., and Gardes-Albert, M. (1994) Antioxidant action of *Gingko biloba* extract EGb 761. *Methods Enzymol.* **234**, 462–475
46. Tendi, E.A., Bosetti, F., Dasgupta, S.F., Stella, A.A., Drieu, K., and Rapoport, S.I., (2002) Gingko biloba extracts EGb 761 and biobalide increase NADH dehydrogenase mRNA level and mitochondrial respiratory control ratio in PC12 cells. *Neurochem. Res.* **27**, 4319–4323
47. Luo, Y., Smith, J.V., Paramasivam, V., Burdick, A., Curry, K.J., Buford, J.P., Khan, I., Netzer, W.J., Xu, H., and Butko, P. (2002) Inhibition of amyloid-beta aggregation and caspase-3 activation by the Gingko biloba extract EGb761. *Proc. Natl. Acad. Sci. USA* **99**, 12197–12202

第15回 モノクローナル抗体を用いたポリグルタミン酸化チューブリンの神経細胞内局在

新井孝夫 Takao Arai（東京理科大学理工学部応用生物科学科）
E-mail：takarai@rs.noda.tus.ac.jp／URL：http://www.rs.noda.tus.ac.jp/~takarai/

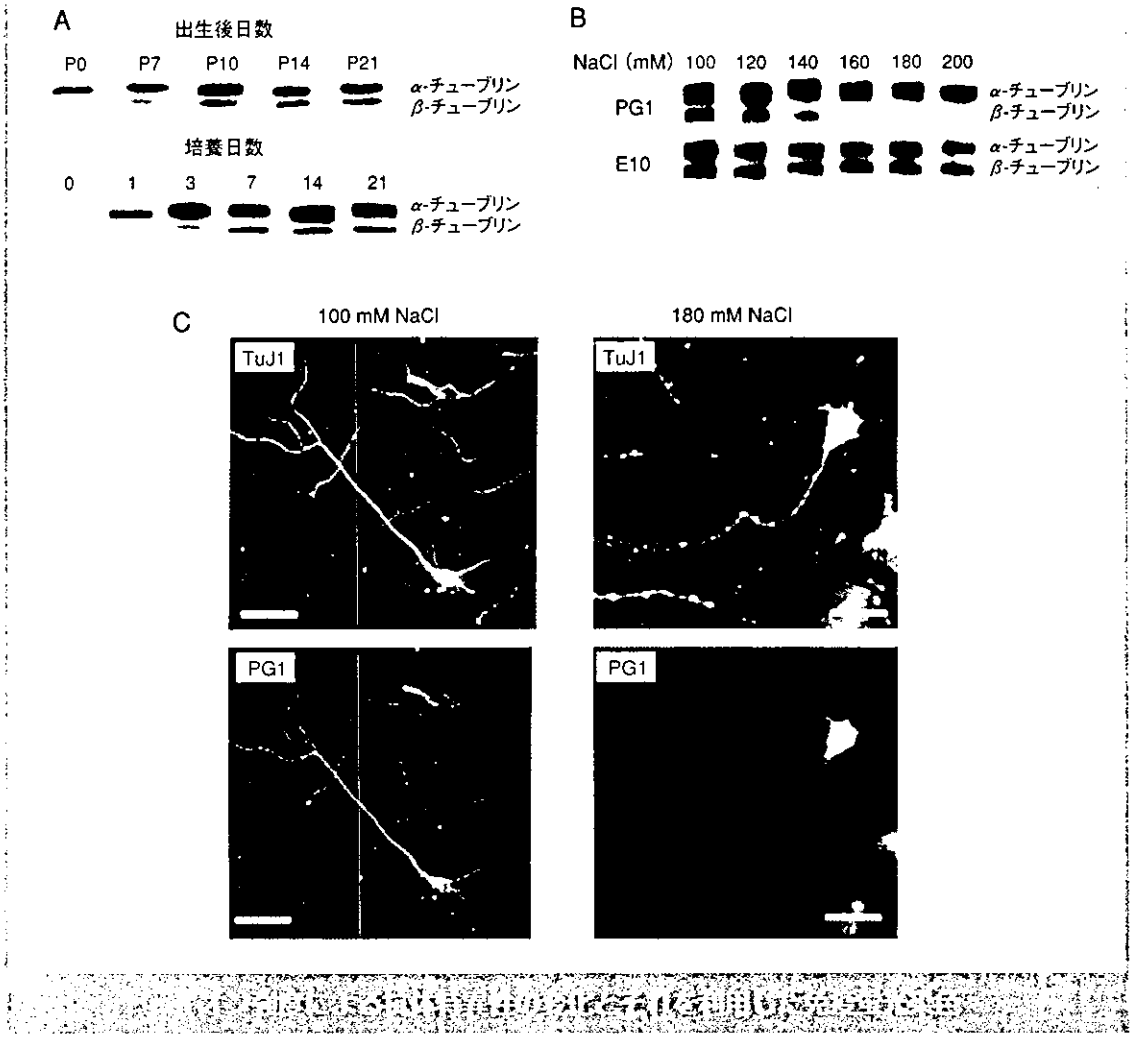

A）発達過程を追ったラット脳およびレチノイン酸存在下培養のラット胎仔脳神経幹細胞におけるチューブリンのポリグルタミン酸化を，抗ポリグルタミン酸化チューブリン抗体PG1により解析した．培養1日後には胎仔脳と同様にα-チューブリンが，3日目以降は成熟脳と同様にα-，β-両チューブリンがこの翻訳後修飾を受けた．B）PG1の反応特異性はNaCl濃度に依存し，高塩濃度ではα-チューブリン特異的であった．C）7日培養の神経幹細胞におけるこの修飾チューブリンの局在を，PG1と抗βIII-チューブリン抗体TuJ1を用いた二重免疫蛍光抗体法で調べた．100 mMと180 mM NaCl条件下における染色性の相違は，神経突起ではβ-チューブリンのみがポリグルタミン酸化されることを示している．スケールバー：50 μm

背　景

α-，β-チューブリンのC末端はグルタミン酸残基の豊富な領域であるが，この領域内のグルタミン酸残基のγ位カルボキシル基に，さらに数個のグルタミン酸残基が付加するポリグルタミン酸化という翻訳後修飾を受ける．モノクローナル抗ポリグルタミン酸化チューブリン抗体の多くは，α-とβ-チューブリンの両者を認識する[1]．多くの臓器や胎仔脳ではα-チューブリンのみがこの修飾を受けているのに対し，成熟脳では両チューブリンが修飾される[2]．現在のところ，この翻訳後修飾を受けたチューブリンの神経細胞内局在の研究は進んでおらず，この翻訳後修飾の果たす役割についての有力な考えも確立されていない．

イメージングが明らかにしたポリグルタミン酸化チューブリンの神経細胞内局在

モノクローナル抗ポリグルタミン酸化チューブリン抗体PG1は，図Aの上に示したように，ラット脳の発達の過程におけるα-，β-チューブリンのポリグルタミン酸化の制御を調べるうえで有用である．また，胎仔脳あるいは成熟脳から神経幹細胞を調製する技術や神経細胞に分化させる培養系は確立されている[3]．そこで，ラット胎仔脳神経幹細胞をレチノイン酸存在下において8ウェルカルチャースライド中で培養し，PG1を用いたウエスタンブロットによりチューブリンのポリグルタミン酸化を調べた．図Aの下に示したように，1日後にはα-チューブリンのみがポリグルタミン酸化され，3日目にはβ-チューブリンの修飾も認められた．β-チューブリンの修飾は，7日目でほぼ一定となった．このことは，この培養系がチューブリンポリグルタミン酸化の研究に有用であることを示している．一方，PG1のα-，β-チューブリンに対する特異性がリン酸緩衝液中のNaCl濃度により変化することを見出した（図B）．すなわち，100 mM NaCl中では両チューブリンを認識したが，180 mM NaCl濃度ではα-チューブリン特異的な反応性を示した．これに対し，同じ抗ポリグルタミン酸化チューブリン抗体E10の場合は，NaCl濃度による反応特異性の変化は起こらなかった．

レチノイン酸存在下で7日培養した神経幹細胞におけるポリグルタミン酸化チューブリンの局在を，この塩濃度変化に依存した抗体特異性の変化を利用して，PG1と神経細胞特異的な抗βⅢ-チューブリン抗体TuJ1を用いた二重免疫蛍光抗体法により観察したのが図Cである．100 mM NaClの染色条件下では細胞体と神経突起の両者が染色されたのに対し，180 mMにおいては細胞体しか染色されなかった．このことは，神経突起においてはβ-チューブリンのみがポリグルタミン酸化されることを示唆している．

翻訳後修飾タンパク質を認識するモノクローナル抗体には，タンパク質特異性の低いものが多い．塩濃度変化によりタンパク質特異性のある反応条件を見出したという本研究結果は，モノクローナル抗体が翻訳後修飾の研究にとって有力な武器となることを改めて示したものと意義づけることができる．

今後の展望と可能性

脳の発達に伴うチューブリンのポリグルタミン酸化の研究から，β-チューブリンのポリグルタミン酸化は神経細胞の成熟と関連すると考えられている．β-チューブリンのポリグルタミン酸化が神経突起において重要な役割を果たしていることを示唆するこの結果は，今後の研究の発展の契機となりうるものである．カチオン性リポソームを用いてモノクローナル抗体を細胞内に導入する技術が開発され，抗チューブリンモノクローナル抗体の導入が細胞増殖を阻害することが示されている[4]．イメージングとこれらの技術を併用することにより，機能解明が大きく進展することが期待される．

〈参考文献〉

1）Wolff, A. et al.：Eur. J. Cell Biol., 59：425-432, 1993
2）Audebert, S. et al.：J. Cell Sci., 107：2313-2322, 1994
3）Takahashi, J. et al.：J. Neurobiol., 38：65-81, 1999
4）Ohuchi, T. et al.：Bioimages, 8：57-64, 2000

Platelet and leukocyte adhesion in the cerebral microvasculature

Mami ISHIKAWA [1,2,3], Eiichi SEKIZUKA [2], John H. ZHANG [4],
Anil NANDA [4] and D. Neil GRANGER [3]

[1]Department of Neurosurgery, Tachikawa Hospital,
[2]Clinical Research Unit of National Saitama Hospital,
[3]Departments of Molecular and Cellular Physiology and [4]Neurosurgery, Louisiana State University Health Sciences Center, Shreveport, USA

Introduction

The adhesion of both leukocytes and platelets to microvascular endothelial cells has been implicated in the pathogenesis of ischemia/reperfusion (I/R) injury and in hypercholesterolemia. It has been shown that I/R elicits an inflammatory response that is manifested as an accumulation of adherent leukocytes and platelets in the cerebral microvasculature. Since platelets can produce inflammatory mediators, such as platelets-derived growth factor, platelet factor 4, thrombospondin and nitric oxide, platelet adhesion may play an important role after I/R. Hypercholesterolemia is known to induce a proinflammatory and prothrombogenic state in the microvasculature of different tissues; however, there has been no documented effort to determine whether the cerebral microcirculation responds to hypercholesterolemia. The objectives of this study were to: 1) assess the platelet and leukocyte adhesion induced in the cerebral microvasculature by middle cerebral artery occlusion (MCAO)/ reperfusion and by hypercholesterolemia, and 2) define the molecular determinants of the prothrombogenic and inflammatory responses in these experimental models.

Material and methods

C57Bl/6J mice were anesthetized and craniotomy was made without cutting the dura matter. Isolated platelets labeled with carboxyfluorescein diacetate succinimidyl ester (CFDASE) were administered intravenously and observed with intravital fluorescence microscopy. Leukocytes were observed following intravenous injection of rhodamine 6G. MCAO was induced for 1 h and after 4 h reperfusion the adhesion of platelets and leukocytes was observed. Without MCAO, platelet and leukocyte adhesion was also examined in mice placed on either a normal diet (ND) or high-cholesterol diet (HCD) for two weeks. In both MCAO and hypercholesterolemia models, some groups were

treated with a monoclonal antibody (mAb) against either P-selectin or GPIIb/IIIa. In another series of experiments, the effects of 30 min MCAO / 4 h reperfusion on platelet and leukocyte adhesion were studied in mice placed on HCD for 1 week.

Results

One hour of MCAO followed by 1 h of reperfusion resulted in the rolling and adhesion of leukocytes in venules, and after 4 h reperfusion, the adhesion of both leukocytes and platelets was detected. While both the P-selectin and GPIIb/IIIa mAbs significantly reduced the adhesion of leukocytes and platelets at 4 h reperfusion, the anti-adhesive effects of the P-selectin mAb were much greater.

When adhesion of ND platelets was monitored in ND recipients, low level interactions were noted. However, when ND platelets were monitored in HCD recipients, greatly elevated levels of platelet adhesion were observed. Similar adhesion responses were noted when HCD platelets were monitored in ND recipients. The increases in leukocyte and platelet adhesion induced by HCD were significantly attenuated after treatment with a mAb against P-selectin, but not GPIIb/IIIa.

Platelet and leukocyte adhesion increased significantly in HCD mice with MCAO/reperfusion, compared to either HCD alone or MCAO alone.

Conclusion

MCAO/reperfusion injury and diet-induced hypercholesteroleima cause the cerebral microvasculature to assume a proinflammatory and prothrombogenic phenotype. Hypercholesterolemia is a major risk factor for the development of ischemic stroke. Our results indicate that antagonists directed against P-selectin may be beneficial in the treatment of stroke, particularly when accompanied by hypercholesterolemia.

(Key Words: platelet, leukocyte, P-selectin, GPIIb/IIIa, cerebral ischemia, reperfusion, hypercholesterlemia)

Soft X-ray imaging of living cells in water: flash contact soft X-ray microscope

Toshikazu Majima

Flash contact soft X-ray microscopy (FCSXRM) is an imaging technology for observing living cells in aqueous conditions with a spatial resolution of several tens of nm. The principle of soft X-ray imaging for living cells is carbon imaging, which provides us with a carbon-density-distribution map of the specimens. Carbon and oxygen have absorption edges in the soft X-ray wavelength range at 4.4 and 2.3 nm, respectively. Between these edges, the photoabsorption cross-section of carbon is about 10 times greater than that of oxygen. Thus, one can obtain soft X-ray images of living cells in water using this wavelength range.

Laser-produced plasma is used as a flash X-ray source. A table-top FCSXRM, named FCSXRM ETL Mark 3, was developed in 1996 for convenient laboratory use of SXRM. The X-ray image of a specimen is recorded on a photoresist polymethyl methacrylate (PMMA) membrane supported on a silicon wafer. The X-ray image is then enlarged by an atomic force microscope (AFM). The practical resolution achieved by the system is about 40 nm, including the tip effect of the AFM. In this article, I discuss the possible roles of the FCSXRM for nanometer-scale imaging of living cells under physiological conditions.

Toshikazu Majima*
National Institute of Advanced Industrial Science and Technology (AIST), 1-1-1 Umezono, Tsukuba, Ibaraki 305-8568, Japan

*Tel.: +81-29-861-5535; Fax: +81-29-861-5540; E-mail: t.majima@aist.go.jp

1. Introduction

The X-ray microscope is an instrument for observing a specimen using X-rays instead of visible light or electron beams [1–4]. X-rays are electromagnetic waves with a wavelength range characterized as being between vacuum ultraviolet rays and γ-rays. X-rays that have longer wavelength, about 50–0.5 nm, are called soft X-rays, and those that have shorter wavelength, about 0.5 nm to 1 pm, are called hard X-rays. The characteristic properties of X-rays compared with visible light and electron beams are as follows:

(1) longer penetration length into materials than electron beams;
(2) shorter wavelength than visible light;
(3) the characteristic absorption spectrum of X-rays is specific to each element.

Nowadays, these characteristic properties of X-rays are used for non-destructive inspection tests in various fields, including medical services, scientific research, and engineering development.

In this article, we will focus on soft X-ray imaging of living specimens in water by a flash contact soft X-ray microscopy (FCSXRM) using laser-produced plasma as a flash X-ray source, and discuss the advantages of flash X-ray exposure for *in situ* observation of living cells with higher resolution than the light microscope and for current scientific research and nanotechnology.

It has been a hard task for the electron microscope to observe living specimens, such as microorganisms and cells cultured in a medium, as it is even for a SXRM without flash exposure of soft X-rays. Soft X-ray imaging requires a considerable number of X-ray photons to obtain a fine X-ray image of the specimen. The number of X-ray photons is great enough to cause thermal denaturalization of the specimen resulting from the X-ray absorption of the specimen itself during the X-ray exposure. Because of this limitation, one should use a flash exposure of soft X-rays to obtain a fine image of specimen in water, although the given X-ray image represents the specimen at the final moment of its life.

2. Advantage of SXRM to observe living specimens

As is well known, more than 95% of the atoms that compose biological specimens

0165-9936/$ - see front matter © 2004 Published by Elsevier B.V. doi:10.1016/S0165-9936(04)00705-8

are oxygen, carbon, nitrogen and hydrogen. These elements are included in macromolecules, such as proteins, lipids, nucleic acids, carbohydrates and water molecules. Of these elements, oxygen, nitrogen and carbon have k-shell absorption edges in the soft X-ray wavelength range. At the wavelength range between the absorption edge of carbon (4.4 nm) and that of oxygen (2.3 nm), the X-ray absorption coefficient of carbon is about 10 times larger than that of oxygen. (Fig. 1) [5]. Using the absorption difference at this wavelength range, which is called the "water window" wavelength range, one can obtain a soft X-ray image of living specimens in water as a carbon-density-distribution map of the specimens. Wolter discussed the possibility of the soft X-ray imaging of biological specimens at the water-window range in 1952 [6]. However, it took a long time to realize soft X-ray imaging of living specimens as a result of several technical problems.

The spatial resolution of a microscope is defined by the distance between two points that can be clearly distinguished using the instrument. It depends on the wavelength of the electromagnetic waves used for observation. In the case of the SXRM using soft X-rays in the water-window wavelength range, the theoretical resolution is a few nm. The practical resolution achieved by SXRMs is, however, several tens of nm. The ultimate aim for the SXRM is to observe living specimens in water with a higher resolution than the light microscope, which is hard for the electron microscope. As mentioned above, the spatial resolution of the SXRM lies between that of the light microscope and that of the electron microscope.

3. Example of soft X-ray image

In a table-top type of FCSXRM, named ETL Mark 3, in AIST in Tsukuba, an X-ray image was recorded on a polymethyl methacrylate (PMMA) membrane (thickness 500 nm) coated on a silicon wafer [7]. PMMA is an X-ray sensitive resist used in applying lithography to production of electronic devices. An X-ray photon absorbed by the PMMA molecule breaks a main chain of the polymer molecule. The dissolution rate of reduced pieces of the PMMA molecules into inorganic solvents is greater than that of the original ones. At the PMMA surface, where the specimens are absent, more PMMA molecules are broken than those at the PMMA surface covered by the specimens. As a result, the dissolution rate of each part of the PMMA surface varies depending on its history during the X-ray exposure. Accordingly, an X-ray image of the specimen is recorded on the PMMA surface as a thin relief. This soft X-ray image recorded on the PMMA surface is then enlarged by an atomic force microscope (AFM) [8,9].

A soft X-ray image of a sea-urchin sperm in sea water was reported by Tomie et al. [8]. The image shown in Fig. 2 is the AFM readout of one soft X-ray image. To stress details of the X-ray image, the z-axis is emphasized compared to the x- and y-axes, and the X-ray image is presented with a mesh display mode. We should notice the thickness of the X-ray image, which is less than 150 nm. In the X-ray image, a sperm head and a flagellum stringing out from the sperm head are clearly visible. Light and electron microscopic investigation of a sea-urchin sperm showed that the sperm head of the sea urchin has a mitochondria with a doughnut-like shape at the rear part of the sperm head [10], and the mitochondrion is a sub-cellular organelle supplying adenosine triphosphate (ATP) molecules for flagella beating. To the rear of the X-ray image, a concave crossing the sperm head is visible, which represents a boundary between the nucleus and the mitochondrion in the sperm head. In soft X-ray imaging, the carbon-density-distribution map of the specimen is projected, thus the boundary of cellular organelles is sometimes represented

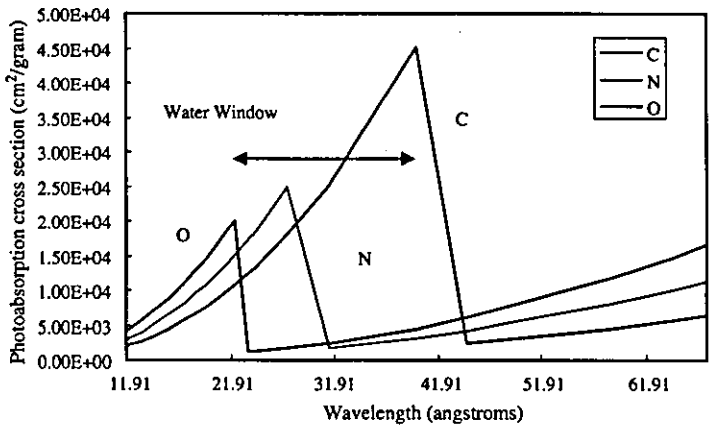

Figure 1. X-ray absorption coefficient of carbon, nitrogen and oxygen.

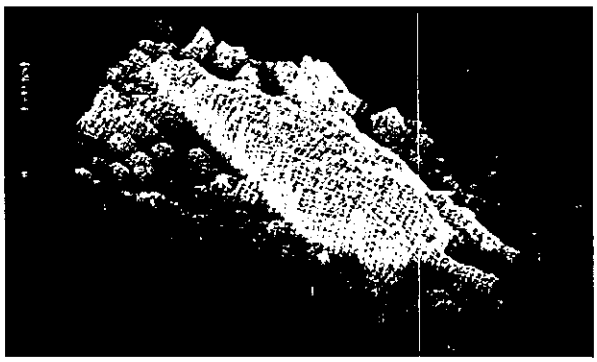

Figure 2. X-ray image of a sea-urchin sperm in seawater enlarged by AFM. The X and Y axes are graduated in μm scale.

in the soft X-ray image as a low carbon-density part of the specimen.

A cross-section of the X-ray image at the mitochondrion measured by the AFM is shown in Fig. 3. The mitochondrion has a doughnut-like shape and the flagellum is stringing out from the central hole of the mitochondrion. The carbon content of the sperm flagellum is not so high as those of the mitochondrion, as shown in Fig. 3. Consequently, the soft X-ray image of the mitochondrion, which is given as a side-on projection of the doughnut-shaped object, shows a concave portion corresponding to the central hole. The cross-section of the X-ray image at the mitochondrion represents a two-peak profile (Fig. 3).

An X-ray image of a bacterial cell is shown in Fig. 4. In some cases, the X-ray image has a large concavity where the carbon density is lower than the background of the bacterial cell body [11]. The diameter of the

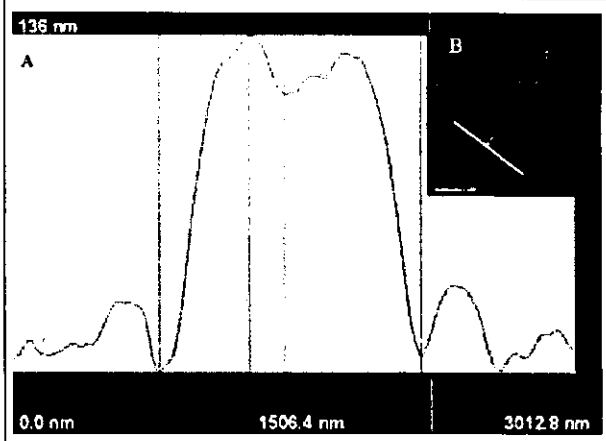

Figure 3. (a) Cross-section of the X-ray image of the sea-urchin sperm at the mitochondria; (b) top view of the X-ray image of the sea-urchin sperm. The cross-section was obtained along the white line.

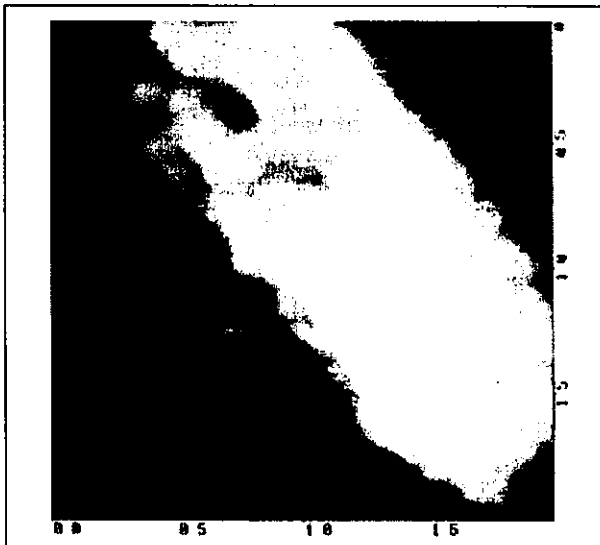

Figure 4. X-ray image of bacterial cell enlarged by AFM. The X and Y axes are graduated in μm scale.

concavity is 500 nm, occasionally rising to as much as 1 μm. Sometimes, a small void in a low carbon-density region is recognized at the center of the concavity. In a bacterial cell, a nucleoid is a sub-cellular structure of the right size to correspond to the concavity on the X-ray image. The nucleoid comprises a large circular DNA molecule containing 4.4 million base pairs [12]. We can estimate the weight of the circular DNA to be 1.9×10^{-15} g assuming an average molecular weight of 260 Da per base pair. The estimated mass density of the nucleoid forming a sphere with a diameter of 550 nm is given as 0.04 g/ml and the specific gravity of the nucleoid with the same volume of water becomes 1.04. A bacterial cell contains 70% water by weight. If we assume that half of the organic molecules are in cellular plasma, the specific gravity of the plasma can be roughly estimated to be (70 + 15)/70 and the specific gravity to be 1.2. In addition, the difference of the ratio of chemical elements in DNA and protein in mammalian sperm [13] and plant cells [14] affects the faintness of the nucleoid in the soft X-ray image relative to the cellular plasma. This also contributes to the concave formation on the X-ray image.

A cryo-electron microscopic image of a thin section of *Escherichia coli* has been reported [15]. The structure of the nucleoid of *E. coli* observed by the cryo-electron microscope is similar to that observed by the SXRM. A small void at the center of the nucleoid is clearly demonstrated, although the center of the nucleoid was drawn as an electron-dense region of the cryo image. Despite the difference of contrast in the two images, these results suggest that the soft X-ray image of the specimen obtained in water resembles the cryo-electron microscopic image.

SXRM provides us with sub-cellular structure of living specimens in water without chemical staining and dehydration of the specimen. The high carbon sensitivity of SXRM at the water-window-wavelength range will be useful for observing gel-like structures rich in water, which is impossible by electron microscopic observation [16,17]. As an example, a soft X-ray image of the cell body of unicellular green alga *Chlamydomonas* sp. is shown in Fig. 5. The cell body including two flagella is presented. Around the cell body, we can recognize a translucent structure in which two flagella are stringing out from the cell body. A gel layer around the cell body is visible.

4. Need for flash exposure of soft X-rays

The major obstacle to obtaining a fine soft X-ray image of a living specimen is the thermal denaturalization of the specimen itself caused by X-ray absorption during the X-ray exposure. In soft X-ray imaging, the energy of X-rays absorbed by carbon atoms in macromolecules in the specimen changes into thermal energy and this raises the temperature of the specimens. Finally, it deforms the specimens, resulting in blurry X-ray images under long X-ray exposure. In the case of SXRM using synchrotron-radiation beams, a few tens of seconds of X-ray exposure is required. The amount of X-ray photons necessary to make an X-ray image with a spatial resolution of 100 nm is at least more than 10^4 times the dose level that causes biological damage to the specimens, and this increases as the spatial resolution increases [18,19]. Because of this damage, application of SXRM using a synchrotron for observation of living specimens in water has not been achieved despite of its usefulness elsewhere in scientific research (e.g., for X-ray diffraction studies of protein molecules). To avoid thermal deformation of the specimens, a cryo SXRM was constructed so that the specimens were embedded in an ice cube chilled by liquid nitrogen [20].

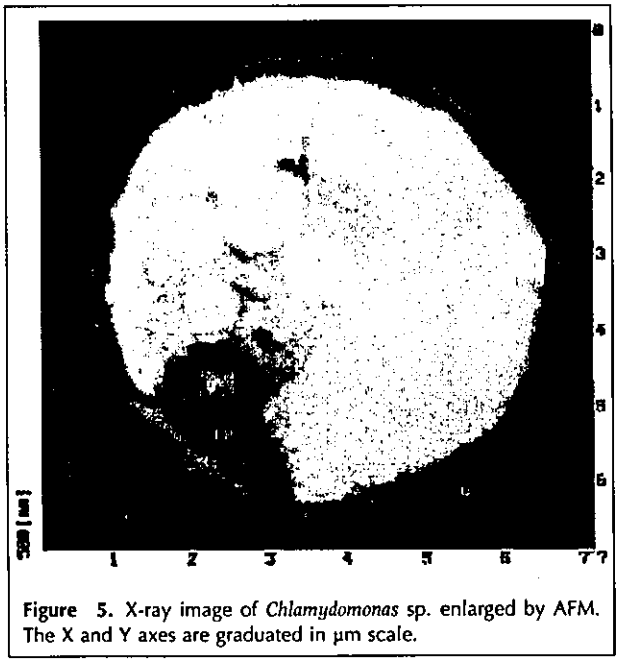

Figure 5. X-ray image of *Chlamydomonas* sp. enlarged by AFM. The X and Y axes are graduated in μm scale.

In order to observe living specimens in water, flash exposure is essential to prevent deterioration of the X-ray image affected by the thermal deformation of the specimens during the X-ray exposure. As mentioned above, the energy of soft X-rays absorbed by the carbon components of the living specimens causes thermal deformation of the specimens. However, these processes require a definite length of time because of the delay in thermal conduction; one can therefore obtain a fine soft X-ray image of specimens using a flash exposure that should be finished before thermal deformation of the specimens can begin. With this technique, fine soft X-ray imaging of living specimens in water has been successful. Flash X-ray exposure of less than 10 ns gives us a successful X-ray image of the specimens free from thermal disturbance, although these X-ray images represent the last stage of life of the living specimens.

5. FCSXRM

The diagram in Fig. 6 represents an outline of the X-ray exposure chamber in our SXRM. In the instrument, a table-top laser is used for plasma production, and the X-ray microscope itself is placed on an optical bench. This enables biologists to use the X-ray microscope in their own laboratories. The X-ray exposure system comprises a pair of nested cylinders; an outer cylinder corresponding to a vacuum chamber for plasma production and an inner cylinder as a sample holder in which living specimens in culture medium are settled on a PMMA chip. Plasma production requires vacuum conditions, and living specimens should be kept under atmospheric conditions. An X-ray window made of a silicon-nitride membrane (0.3 mm square, 200 nm thick) supported on a silicon wafer (10 mm square, 200 μm thick) separates the outer chamber and the sample holder. The X-ray window is installed inside the top of the inner chamber and is sealed by coating with red nail varnish. It works as both an X-ray permeable window and a pressure bulkhead between the two cylinders.

A second harmonic light pulse (532 nm) from a Nd:YAG laser is used to produce the plasma that works as a flash soft X-ray source. Using an optical lens (not shown in the diagram), the light pulse is focused on a target made of yttrium foil located at the top of the sample holder, and the plasma is produced. Then, soft X-rays irradiate the specimens on the PMMA membrane

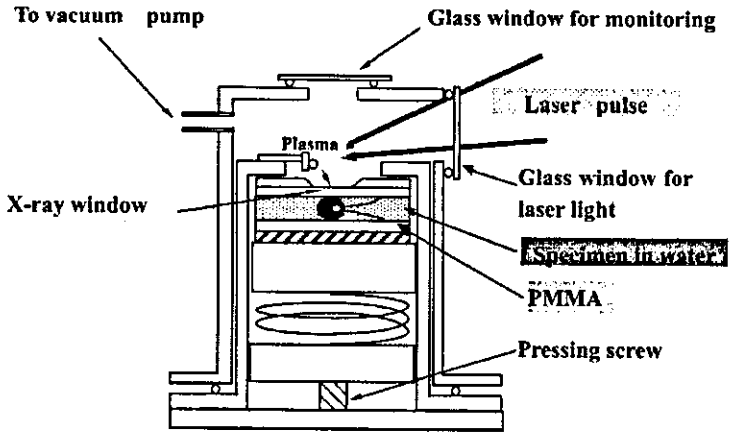

Figure 6. Cross-section of the X-ray exposure chamber and the principle of recording.

through the X-ray window. Specimens just under the X-ray window are irradiated by the X-ray flash. After the irradiation, the specimens on the PMMA membrane are washed out to clean up the surface of the PMMA chip.

The PMMA chip is chemically developed in a 1:1 (v/v) mixture of methyl isobutyl ketone and isopropanol. Chemical development generates the X-ray image of the specimen on the PMMA surface as a thin relief of the full size of the specimen. The X-ray image on the PMMA surface is enlarged by an AFM. Application of AFM is convenient not only for observing the shape of the X-ray image by two-dimensional enlargement, but also for obtaining of the carbon-density profile of the specimens by analyzing the height of the X-ray image. The relative thickness of the X-ray image, more properly the depth dug down by the chemical development, contains information on the carbon-density profile in the specimen along the X-ray projection.

6. Other X-ray microscopes

Apart from the FCSXRM mentioned above, various other types of X-ray microscopes are constructed today [1,3,4]. These are categorized according to:

(a) the X-ray source;
(b) the presence or absence of imaging optics;
(c) the recording medium for the X-ray image.

Synchrotron radiation, laser-produced plasma and X-ray tube are typical X-ray sources.

Imaging optics is used for enlargement of the X-ray image. A zone plate, which is a kind of circular diffraction grating for accumulating diffracted X-rays at the same point on an optical axis, works as a lens for X-rays. A reflection mirror for X-rays is also used to focus X-rays to magnify the X-ray image. Without imaging optics, a projection-type X-ray microscope is available using a point source of X-rays [21].

The recording medium is another important item of X-ray microscopy. X-ray resists, such as PMMA and EPR (an epoxy novolac-based chemically amplified photoresist [22], or a CCD camera are used.

7. Past and future

The history of X-ray microscopy is much longer than that of electron microscopy. Not long after the discovery of X-rays in 1895, several efforts were made to develop X-ray microscopes. There were several barriers to obtaining an X-ray image:

(1) the recording medium for the X-ray image;
(2) an X-ray source brilliant enough for imaging;
(3) an enlargement technique for the X-ray image.

At the beginning of the last century, the technological background of X-ray microscopy had not matured enough to make an X-ray microscope possible. The innovation of the cathode ray tube in the 1930s accelerated the development of electron microscopy. As is well known, the electron microscope has become an essential instrument to observe nanometer-scale objects in various fields of current science and technology.

The development of integrated circuits (IC) in the 1980s reactivated many research fields related to construction of the X-ray microscope. Lithography, a technology for microfabrication, played important roles in the development of modern X-ray microscopy. Microfabrication enables us to develop a zone plate that works as a lens for X-rays and research into the X-ray microscope with imaging optics has become mainstream, coinciding with the construction of synchrotrons around the world.

The development of the high-power laser also activated research into the X-ray microscope at the same time. In the 1980s, pulsed plasma was suggested as a soft X-ray source for X-ray lithography and X-ray microscopy [23–25] and a laser-produced plasma is considered to be a convenient flash X-ray source for soft X-ray microscopy [26]. The lifetime of the laser-produced plasma ranges from several hundreds of picoseconds to several tens of nanoseconds, depending on the duration of the laser pulse used. Using plasma for less than 10 ns, one can obtain a fine X-ray image by FCSXM without thermal deformation of the specimen [27].

A laser-induced plasma is strong enough to supply photons necessary for fine X-ray imaging within a few nanoseconds. A table-top type of X-ray microscope for a small laboratory provides information that is hard to obtain by visible light or electron microscopes.

Recent developments in the biosciences require us to observe living cells *in situ* with higher resolution. Application of the FCSXRM to tissues, where observation of objects in water is essential to understand the primary nature and/or structure of the objects, will open up a new field of nanometer-scale imaging in water.

Acknowledgements

I thank Professor Hideaki Shimizu of Kagawa University for reading the manuscript critically, and I am grateful to my colleagues for sharing their results.

References

[1] J. Kirz, C. Jacobsen, M. Howells, Quart. Rev. Biophys. 28 (1995) 33.
[2] T. Majima, H. Shimizu, T. Tomie, BioImages 7 (1999) 59.
[3] C. Jacobsen, Trends Cell Biol. 9 (1999) 44.
[4] J. Susini, D. Joyeux, F. Polack (Eds.), X-ray Microscopy, EDP Sciences, Paris, France, 2003.
[5] B.L. Henke, P. Lee, T.J. Tanaka, R.L. Shimabukuro, B.K. Fujikawa, At. Data Nucl. Data Tables 27 (1982) 27.
[6] H. Wolter, Ann. Physik. 10 (1952) 94.
[7] H. Shimizu, T. Tomie, T. Majima, A.D. Stead, T.W. Ford, E. Miura, M. Yamada, T. Kanayama, in: J. Thieme, G. Schmahl, D. Rudolph, E. Umbach (Eds.), X-ray Microscopy and Spectroscopy, Springer, Berlin, Germany, 1998, pp. I–157.
[8] T. Tomie, H. Shimizu, T. Majima, M. Yamada, T. Kanayama, H. Kondo, M. Yano, M. Ono, Science (Washington, DC) 252 (1991) 691.
[9] R.A. Cotton, M.D. Dooley, J.H. Fletcher, A.D. Stead, T.W. Ford, in: C.J. Jacobsen, J.E. Trebes (Eds.), Soft X-ray Microscopy, Proc. SPIE, 1741, 1993, p. 204.
[10] G. Giudice, The Sea Urchin Embryo, Springer, Berlin-Heidelberg, Germany, 1986.
[11] T. Majima, H. Shimizu, T. Tomie, E. Miura, T. Kanayma, M. Yamada, in: J. Thieme, G. Schmahl, D. Rudolph, E. Umbach (Eds.), X-ray Microscopy and Spectroscopy, Springer, Berlin, Germany, 1998, p. II-261.
[12] L.C. Klotz, B. Zimm, J. Mol. Biol. 72 (1972) 779.
[13] X. Zhang, R. Balhorn, J. Mazrimas, J. Kirz, J. Struct. Biol. 116 (1996) 335.
[14] A.D. Stead, R.A. Coton, J.A. Goode, J.G. Duckett, A.M. Page, T.W. Ford, J. X-ray Sci. Technol. 5 (1995) 52.
[15] J.A. Hobot, W. Villiger, J. Escaig, M. Maeder, A. Ryter, E. Kellenberger, J. Bact. 162 (1985) 960.
[16] T.W. Ford, A.M. Page, H. Shimizu, T. Tomie, T. Majima, A.D. Stead, in: J. Thieme, G. Schmahl, D. Rudolph, E. Umbach (Eds.), X-ray Microscopy and Spectroscopy, Springer, Berlin, Germany, 1998, p. II-173.
[17] T. Majima, H. Shimizu, T. Tomie, E. Miura, T. Kanayama, M. Yamada, in: D.L. Farkas, B.J. Tromberg (Eds.), Functional Imaging and Optical Manipulation of Living Cells, Proc. SPIE, 2983, 1997, p. 81.
[18] T.W. Ford, A.M. Page, G.E. Foster, A.D. Stead, in: C.J. Jacobsen, J.E. Trebes (Eds.), Soft X-ray Microscopy, Proc. SPIE, 1741, 1993, p. 325.
[19] P.M. Bennett, G.F. Foster, C.J. Buckley, R.E. Burge, J. Microsc. 172 (1993) 109.
[20] G. Schneider, R. Niemann, P. Guttmann, D. Rudolph, G. Schmahl, Synch. Rad. News 8 (1995) 19.
[21] H. Yoshimura, D. Shoutsu, T. Horikoshi, H. Chiba, S. Kumagai, T. Mitsui, J. Electron Microsc. 49 (2000) 621.
[22] C. Cefalas, E. Sarantopoulou, Z. Kollia, P. Argitis, E. Tegou, T.W. Ford, A.D. Stead, B.N. Danson, D. Neely, S. Kobe, Mater. Sci. Eng. C 23 (2003) 105.
[23] J. Perlman, J.C. Riordan, J. Vac. Sci. Technol. 19 (1981) 1190.
[24] J. Bailey, Y. Ettinger, A. Fisher, Appl. Phys. Lett. 40 (1982) 33.
[25] T.W. Ford, A.D. Stead, C.P. Hills, R.J. Rosser, N. Rixvi, J. X-ray Sci. Technol. 1 (1989) 207.
[26] R. Feder, J.L. Costa, P. Chaudhari, D. Sayre, Science (Washington, DC) 212 (1981) 1398.
[27] H. Shimizu, T. Majima, T. Tomie, K. Miura, M. Yamada, T. Kanayama, in: J. Thieme, G. Schmahl, D. Rudolph, E. Umbach (Eds.), X-ray Microscopy and Spectroscopy, Springer, Berlin, Germany, 1998, p. II-267.

RADIOISOTOPES, 53, 245-256 (2004)

連載講座

放射線イメージング技術の最前線（第7回）

密着型フラッシュ軟X線顕微鏡†

眞島利和，雨宮邦招*

独立行政法人産業技術総合研究所　光技術研究部門・ライフエレクトロニクス研究ラボ
305-8568　茨城県つくば市梅園 1-1-1　中央第二
*東京大学大学院工学系研究科システム量子工学専攻
113-0032　東京都文京区弥生 2-11-16

Key Words：X ray microscope, laser plasma, bioimaging, boron neutron capture therapy

1. はじめに

ヒトをはじめとするいくつかの代表的な動植物のゲノムの塩基配列が解読され，遺伝子産物の同定とその機能解析が新たな研究課題として注目されている。このため，従来はin vitroで行われてきた光学顕微鏡による一分子観察も，タンパク質の具体的な機能発現の場である細胞内での一分子観察へと研究の先端が移りつつある。生きている細胞を，より高い時間的・空間的分解能で観察する手段が求められている。

従来，生物の微細構造を観察する手段として光学顕微鏡や電子顕微鏡が用いられてきた。現在では，原子間力顕微鏡（AFM）などのプローブ顕微鏡も使われ始めている。電子顕微鏡との比較でみると，光学顕微鏡の特徴は水の中で生きている生物試料を観察できることにある。光学顕微鏡の分解能は可視光域の短波長側の波長で制限される。これに対して，観察に電子線を用いる電子顕微鏡は，分解能は高いが試料を固定・脱水したのち樹脂に包埋し超薄切片に加工しなければならず，生きている試料をそのまま観察することはできない。このため，ポストゲノム時代のバイオイメージングの課題として，GFP（Green Fluorescent Protein 緑色蛍光タンパク）など各種の蛍光ラベルや量子ドットなどを用いた一分子観察法をはじめとして，生きている細胞の微細構造や機能を時間的・空間的に高分解能で観察する手法が求められている。

本稿で扱う軟X線顕微鏡は，軟X線を用いて生物試料の炭素イメージングを行い，水中で生きている生物試料の内部構造を，光学顕微鏡と電子顕微鏡の中間程度の高分解能（数十nmオーダー）で観察することができる装置である。図1に生物試料のX線像の具体例を示した。

生物を構成している主な元素の組成は，酸素65%，炭素18%，水素10%，窒素2.5%など，軽元素が95%以上である。これらの軽元素は，生体に豊富に含まれている水や，タンパク質，脂質，糖質，核酸などとして生体を構成している。生物を構成している軽元素のX線吸収特性をみると，酸素の軟X線吸収端が2.4 nm，炭素の軟X線吸収端が4.3 nmに位置している。

---

†The Front of Radiation Imaging Technique(7). Flash Contact Soft X-ray Microscope. Toshikazu MAJIMA and Kuniaki AMEMIYA*: Photonics Research Institute & Life Electronics Laboratory, National Institute of Advanced Industrial Science and Technology (AIST), AIST Central 2, 1-1-1, Umezono, Tsukuba-shi, Ibaraki Pref. 305-8656, Japan, *Department of Quantum Engineering and System Science, University of Tokyo, 2-11-16, Yayoi, Bunkyo-ku, Tokyo 113-0032, Japan.

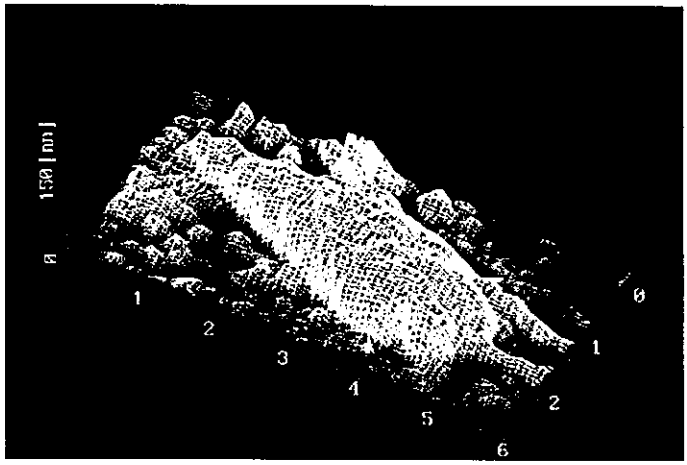

図1 ウニ精子の軟X線顕微鏡像
AFMで読み出したX線像は，厚み方向には拡大率を大きくして，形状が分かりやすいようにメッシュをかけて表示してある。XY軸のスケールはμm，Z軸はnmである

図2に示したように，これらの吸収端の間の波長領域では，炭素の軟X線吸収率が酸素の軟X線吸収率をほぼ1桁上回っている。すなわち水，H_2Oは炭素に吸収されやすい波長の軟X線をよく透過させるという意味で，この波長領域は，「水の窓」と呼ばれている。

酸素と炭素を吸収の差により区別できるこの波長領域の軟X線を用いると，タンパク質をはじめとする有機物に含まれている炭素の密度分布をコントラストよく画像化したものとして生物試料の軟X線像が得られる。本稿では，筆者らが研究・開発を行ってきた密着型フラッシュ軟X線顕微鏡，ETLⅢの概要とその応用について述べる[1)-5)]。

2. 密着型フラッシュ軟X線顕微鏡

2·1 装置の概要

この装置は，レーザー生成プラズマをフラッシュ軟X線源とするX線顕微鏡である。適切なエネルギーを持った可視域の単パルスレーザー光を，凸レンズでイットリウム箔片表面に集光すると，表面温度が局所的に急激に上昇しプラズマが生成される。この短寿命のプラズマをフラッシュ軟X線源として用いる。

密着型のX線顕微鏡の持つ利点は，試料をX線像の記録媒体となるX線感光薄膜上に密着して置くため，X線を結像させるためのフレネルゾーンプレートや多層膜ミラーなどのX線光学素子が不要で，これらを用いる結像形のX線顕微鏡と比較して装置の構成がシンプルな点である。見方を変えると，密着型フラッシュ軟X線顕微鏡法は，培養細胞などの生きている生物試料を転写マスク代わりに用いたX線リソグラフィーと見ることもできる。

筆者らが用いている卓上タイプの密着型フラッシュ軟X線顕微鏡システムは，1) パルス光を供給するNd:YAGレーザー，2) プラズマ生成と試料への露光を行うX線露光装置，3) 露光されたX線記録媒体の現像に用いる微分干渉顕微鏡，4) 得られたX線像を拡大読み出しする原子間力顕微鏡AFMから構成されている。

露光装置の概念図を図3に示した。真空チェンバー内で生成されたプラズマから放射される軟X線を大気圧中に保持された生物試料に照射するために，レーザーからのパルス光を図に

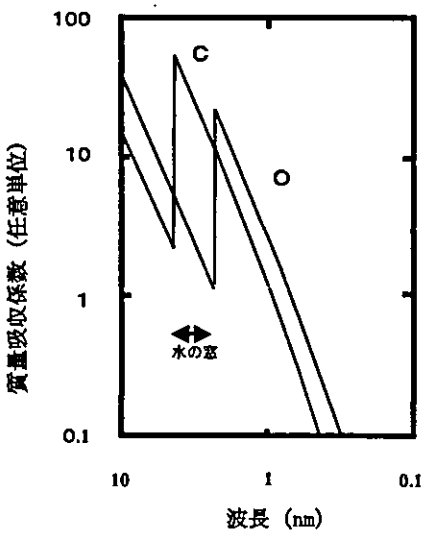

図2　炭素と酸素の軟X線吸収係数の波長依存性

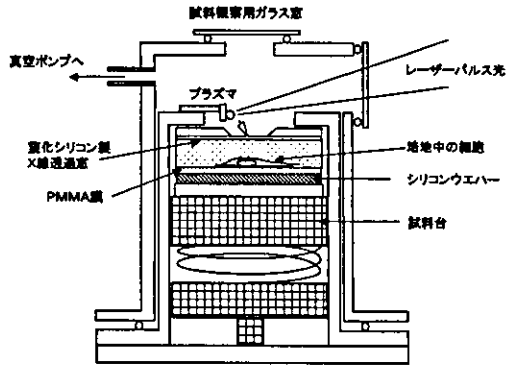

図3　X線露光装置の概念図

は示されていない凸レンズで集光して露光装置内の真空部分に設置したイットリウム箔片にあて，プラズマを発生させる。筆者らの装置では，3 nsの時間幅を持つパルス光を用いているので，約3 ns間のフラッシュX線露光になる。プラズマから出てくる軟X線のスペクトルは，用いる金属によって異なる。イットリウムを用いた場合，プラズマから放射されるX線が先に述べた「水の窓」の波長領域の軟X線成分を多く含むことから，この装置では金属ターゲットとしてイットリウムを用いている。真空チェンバーと試料ホルダーとの間は，試料ホルダー上部に取り付けられた窒化シリコン薄膜製のX線窓により隔てられている。試料は，X線感光性のポリメチルメタクリレートPMMA薄膜をシリコン基板表面にコーティングしたPMMAチップ上に培地ごと置かれている。軟X線露光のために試料を露光装置にセットした状態では，試料ホルダー上部に取り付けられたX線窓とPMMAチップとの間に挟まれた状態になっている。このとき窒化シリコン薄膜は，軟X線を透過させる窓材として機能するとともに，真空に保たれているプラズマ発生部位と大気圧に保たれている試料とを隔てる圧力隔壁としても機能している。

X線露光の結果，露光された試料の等身大の影絵として，試料の炭素密度分布を反映した軟X線像がPMMA薄膜に記録される。X線を吸収すると，PMMA分子の主鎖が切断され断片化される。分子量の小さくなったPMMA断片は，断片化されていない分子と比較して有機溶媒に対する溶解速度が速くなる。このため，露光後にPMMA表面に残っている試料の残滓を取り除いたのち有機溶媒で現像すると，試料の軟X線吸収の度合いを反映した凹凸のある，二次元的には実物大のレリーフ像が軟X線像として得られる。このレリーフ像の形状をAFMで観察すると試料の拡大X線像が得られる（図4）。

乾燥させた生物試料を用いた密着型X線顕微鏡法は，従来からレーザー生成プラズマ以外にもシンクロトロン放射光を光源に用いた軟X線顕微鏡で使われていたが，PMMA上に記録されたレリーフ像のレプリカを作製し，電子顕微鏡でこれを観察する方法がとられていた。この方法では，レプリカの二次元的な形態に関する情報は簡単に得られるが，軟X線顕微鏡法にとって本質的に重要である試料の厚み方向の炭素の分布情報をPMMA上の凹凸から定量的に読み出すことは難しい。この点を改良するた

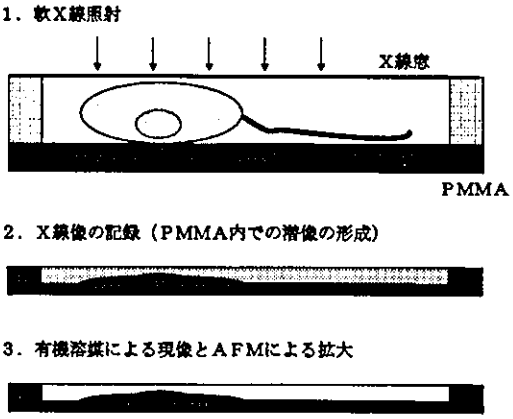

図4 X線像の形成過程

め，X線像の二次元的形態とX線像の高さ方向の情報を同時に読み出す方法として，AFMを用いたX線像の拡大読み出しを行った。AFMでX線像を読みとることにより，PMMA上に記録されたレリーフの高さ方向の情報を正確に読み出すことが可能になった。

2･2 フラッシュ撮影法の意義

生物試料の軟X線顕微鏡観察において問題となるのは，試料の熱変性である。鮮明なX線像を得るには一定量のX線のフォトンが必要であるが，その線量はX線照射によって生物試料が損傷を受けるとされる線量の10^4倍以上になる。生体構成元素の炭素に吸収されやすい波長の軟X線を照射するため，試料に吸収されたX線のエネルギーは最終的には熱エネルギーとなり，試料の熱変性・膨張・変形を引き起こす。露光時間が長いとこれらの変化は，X線像の記録中に起きることになり，X線像を乱す。後述するように，X線顕微鏡にはさまざまなタイプのものがあり，X線源もレーザー生成プラズマ以外にも例えばシンクロトロン放射光が用いられている。シンクロトロン放射光を光源とする場合，照射するX線の波長選択性は高いが，X線像を得るために必要なフォトン数を稼ぐには露光時間を長くする必要があり，露光中に生じる試料の熱変性によるX線像の乱れは避けられない。これを避けるために，氷中に封入した試料に露光するなどの工夫が行われた[6]。しかしこの方式では，生きて動いている生物試料は観察できない。

これに対してレーザー生成プラズマを軟X線源に用いるとフラッシュ露光ができるため，熱変性による試料の変性・変形により生じるX線像の乱れを避けることができる。例えば筆者らが用いている装置では，パルス幅3 nsの単パルス光でプラズマを生成しているため，プラズマの寿命も同程度であり，X線露光は3 nsで終了する。露光による試料の熱変性が始まるのは，用いている露光条件下ではX線露光後20 ns前後からであるので，筆者らの装置でも露光後の試料の熱変性・変形は避けられないが，3 ns間のフラッシュ露光を行えば試料の熱変性が起きる前にX線像の記録を終えることができる。このため，軟X線による生物観察においてはフラッシュ露光は不可欠である。

3. 生物試料の観察

密着型フラッシュ軟X線顕微鏡による生物試料の観察例として，羊保存血液の軟X線顕微鏡像を示す（図5）。円盤状で中央部分が窪んでいる赤血球に特徴的な形状が軟X線像にも現れている。X線像の上部の平らなところは，X線窓を支えるシリコンウエハーの枠の部分の影である。枠の近くに見られる赤血球が重なり合っている箇所では，軟X線の投影方向に対して炭素密度が高くなるために，X線像では重なり合った部分がレリーフの厚みの違いとして表われている。このように軟X線顕微鏡像は試料の炭素密度の違いを敏感に検出できるので，露光条件や現像条件を規格化できれば，X線像を比較して定量的な議論ができる。

大きな試料を観察した例として，ニワトリ胚の後根神経節（Dorsal Root Ganglion）の神経細胞を初代培養したものの軟X線像を図6(a)に示した。この例では，PMMA付シリコン基